THE GENERALIZED USE OF INTEGRATED MAGNETICS

AND ZERO-RIPPLE TECHNIQUES IN SWITCHMODE POWER CONVERTERS

Gordon (Ed) Bloom

Rudy Severns

e/j BLOOM associates

Siliconix, inc.

Abstract

Methods are presented that allow the discrete transformers and inductors of switchmode power converters to be unified in single magnetic structures. It is demonstrated that unified magnetics and zero ripple operation are general phenomena applicable to all types of switchmode power converters.

1 INTRODUCTION

Seemingly, a day does not pass now without an announcement of a new advance in microcircuit technology, bringing us closer to the age of ultra mininaturation of electronic products. For those of us who must design and develop power processing systems it is a time of frustration and reflection, for as product sizes shrink, so must their power conditioners.

Twenty-five years ago, when the sizes of electronic systems were measured in terms of room dimensions, their power supplies could afford to be large. Today, with electronic products, such as calculators smaller than the dial of a watch, the power supply subsystems are often as large or larger than the electronics. Another example is the personal computer, where power supply areas often occupy up to 50% of enclosure volume, with a cost approaching 45% of product price.

In a concerted effort to reduce power supply sizes, recent years have seen switchmode conversion and processing designs pushed higher and higher in operating frequency. Theoretically, at least, converters with high switching rates implies that their circuits will have smaller magnetic components. There are however, very practical limits to the size reduction obtainable from high frequency operation [1].

There is little disagreement among power converter designers that the magnetic parts of any switchmode design are the major contributors to supply cost, weight, and size. For these reasons, it is not uncommon for designers to select converter approaches that have a minimum magnetic content, even though, in many cases, one with more magnetic components would be more suitable from an overall circuit performance standpoint.

Realizing that moving to higher switching frequencies to reduce magnetic size has practical boundaries, designers are now turning to another avenue of investigation - magnetic integration. This rather innovative-sounding, but accurate, term is used to describe magnetic design techniques whereby various inductive and transformer elements of a power converter can be combined on a single core structure.

If one accepts the above definition of magnetic integration as applied to switchmode DC-to-DC power converters, then two converter topologies can be readily identified as integrated magnetic circuits, namely, the buck-boost-derived flyback converter and a special variation of the "boost-buck-derived" 'Cuk converter'[2].

Both of these circuits, together with their discrete magnetic counterparts, are shown in the lower portions of Figure 1. In the case of the flyback converter, the required inductance for energy storage is simply "built-into" the isolation transformer by proper choice magnetization inductance. Thus, the transformer of the flyback converter serves two important purposes - as an isolation element for input and output grounds and as a means of primary energy storage for supplying load power needs. In the case of the integrated-magnetic version of the transformer-isolated 'Cuk Converter, its single magnetic houses all inductive functions of the converter and, by selecting proper amounts of mutual inductance that exist between windings, input and output ripple current magnitudes can be controlled, and even be reduced to zero in special instances [3]! Both the buck-boost converter and its dual circuit, the 'Cuk converter, can be evolved from the appropriate cascade arrangements of basic buck and boost circuits, as demonstrated in [2]. It is interesting to note that integrated—magnetic versions of isolated buck-boost and Cuk converters are perfectly feasible and well-documented circuit possibilities, but little is publicly known about similar integration methods for transformer-isolated versions of their parent circuits, as visually emphasized by the vacant sections of Figure 1.

In this paper, we will explore design techniques for the integration of the transformer and inductive components of buck and boost-derived converter topologies. To set the stage for this examination, a brief introductory section on basic electromagnetic modeling and analysis is included. Discussions of magnetic integration of the inductive components of a forward converter are then presented, with extensions for reducing the output ripple current significantly by external means. By duality integrated-magnetic boost converter circuits are then evolved and extensions illustrated for input ripple current reductions.

Integrated-magnetic "push-pull" DC-to-DC converter structures are then examined, including one based on a special variation of the Weinberg circuit. Results of laboratory tests of a representative integrated magnetic converter are then shown, followed by discussions of small-signal averaged modeling for stability and control analysis.

2 TOOLS FOR MAGNETIC CIRCUIT MODELING

Integrated magnetics for converters brings to mind a picture of magnetic structures that are highly complex and unwieldly from design, analysis, and construction viewpoints. To some degree, this concern is understandable, for most engineers today are only familiar with magnetic design methods that address inductors and transformers as individual converter components. Just the thought of having to deal with a magnetic assembly with more than one major flux path is often a deterrent to an engineer to attempt such a design.

The attitude of designers in this regard is now changing. However, for many converter designers, the tools to proper design and model integrated-magnetic components have been unused over the years. Thus, before beginning the

exploration of integrated-magnetic buck and boost converters, it is worthwhile to digress briefly and review some not-so-familiar electromagnetic fundamentals and magnetic circuit modeling methods using electric circuit analogs. For those readers interested in a more comprehensive review than the one to follow, reference [4] is highly recommended.

Recall that the similarity between Kirchoff's voltage and current laws for linear electric circuits and Ampere's circuital laws related to magnetomotive force and flux continuity in linear magnetic circuits permit the use of electric circuit analogs for analysis purposes. Such analysis makes voltage, v, analogous to magnetic potential F; current, i, analogous to magnetic flux, Ø; electrical resistance, R, analogous to magnetic reluctance, R. Furthermore, because the electric circuits derived by the use of these analogs are linear, they can be manipulated into even more useful forms by established duality relationships [5]. Transformation by duality then produces electric circuit models that relate magnetic reluctances, R's, to inductances, L's; flux linkages in windings, λ 's, to voltages, v's; and flux levels in magnetic paths, Ø's, to currents, i's.

The rate of change of flux with time within a coil of wire (with or without a ferromagnetic core) of N turns can be related to λ , as:

$$v = \frac{d\mathbf{h}}{dt} = N \frac{d\mathbf{p}}{dt} = L \frac{d\mathbf{i}}{dt} \tag{1}$$

by Lenz's and Faraday's Law. As shown in (1), a similar relationship can be stated in terms of the inductance (L) of the coil and the instantaneous current (i) thru it. In the case of a single coil of wire, is the measure of flux linkage within the core produced by self-induction. In an instance where there are multiple coils with common magnetic paths, the total flux linkage of one coil would be the sum of that produced by self-induction plus those produced by mutual interaction, or mutual induction, with the others.

The magnetomotive force, F, of an excited coil of wire (with or without a ferromagnetic core) is defined as the product of the instantaneous current through it, i, and the number of turns, N, of the coil. In equation form, F can be directly related to magnetizing force, H, and its magnetic path length, 1, as:

$$F = Ni = H1 \tag{2}$$

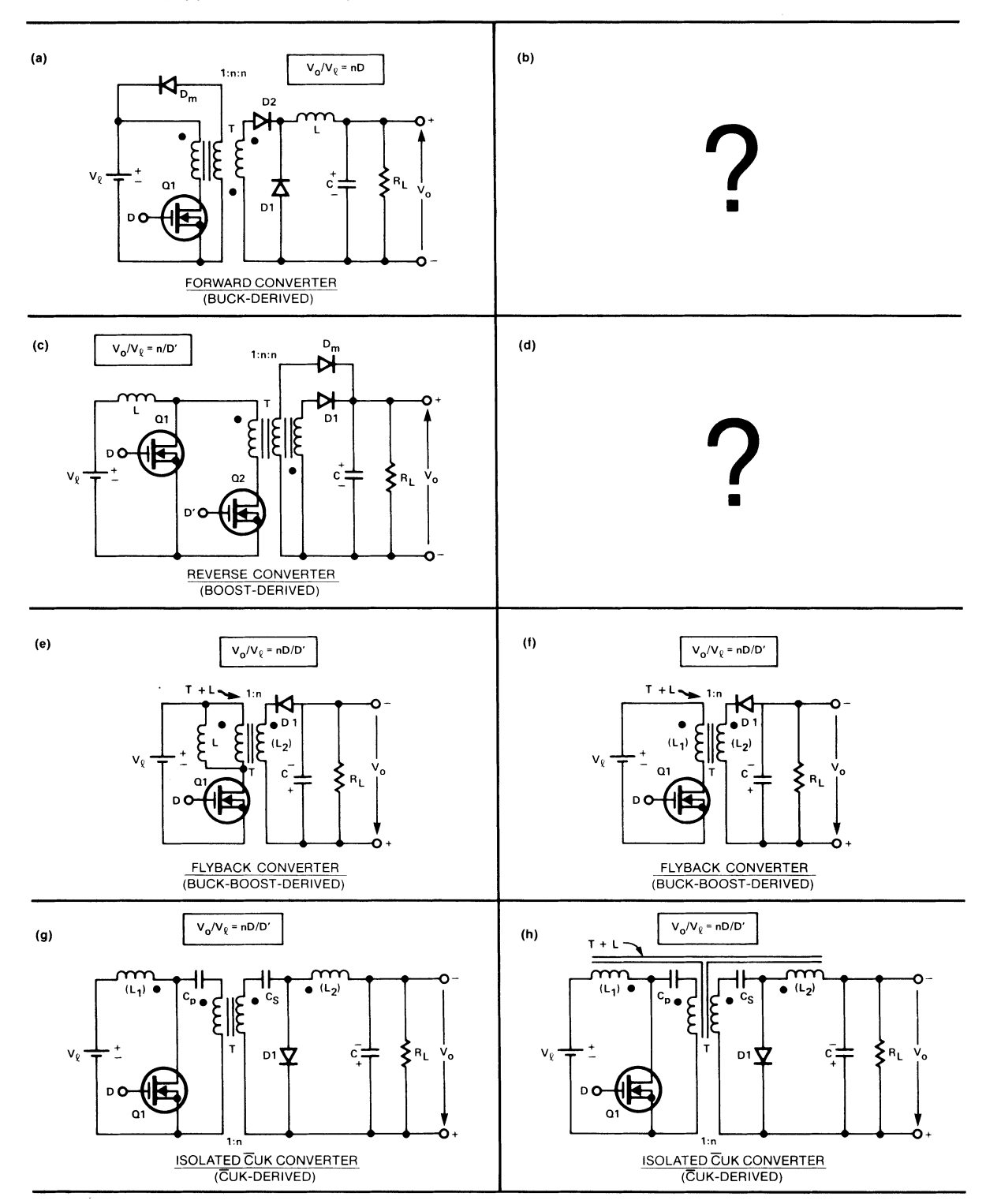


Figure 1 Discrete and integrated-magnetic converter possibilities - what about the forward and reverse designs?

The **self-inductance**, L, of a single coil of wire of N turns, can be equated to the rate of change of flux with current from (1) as:

$$L = N \frac{d\mathbf{g}}{di}$$

Assuming that a linear relationship between flux level and magnetizing force is always maintained, R can be defined as the ratio of a change in F produced by a change in 0. From (2) and (3), reluctance can be expressed in terms of inductance as:

$$R = \frac{dF}{dB} = N \frac{di}{dB} = \frac{N^2}{L}$$
 (4)

Reluctance can also be expressed in terms of related magnetic path length, cross-sectional area of the magnetic material, $^{\rm A}{}_{\rm C}$, and the **permeability**, u, of the path in question. If $^{\rm A}{}_{\rm C}$ is uniform in value throughout the path, then:

$$R = \frac{1}{\mu Ac} = \frac{1}{P} \tag{5}$$

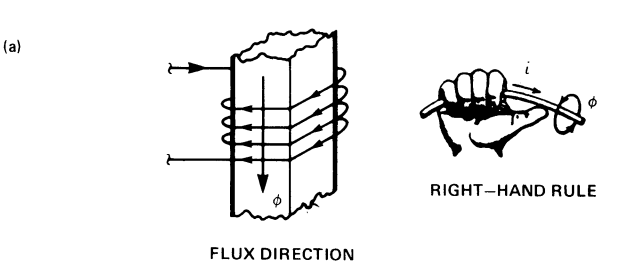
where P is defined as material permeance, the reciprocal element of reluctance.

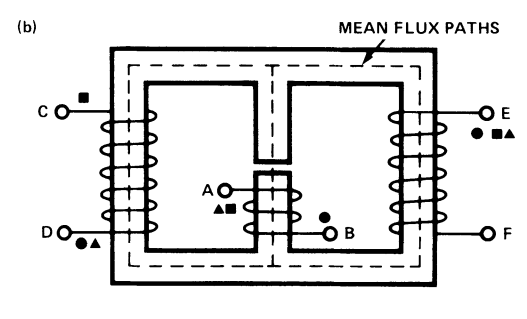
In magnetic circuits, arrows are used to indicate the assumed directions of winding currents, rather than polarity marks for magnetomotive forces (often shortened to "mmfs"). The most popular method for determining flux direction is the "right-hand rule" illustrated in Figure 2(a). With the right hand positioned as shown, the flux direction will be indicated by the direction of the curvature of the fingers. Note that the thumb must be pointed in the assumed direction of winding current when making this determination.

In representing multi-winding magnetic circuits in electric circuit diagrams, it is customary to use **dot notation** to convey the voltage polarity relationships of each winding relative to the others, as shown in Figure 2(b). Three basic rules are followed in the "dotting" of windings:

RULE 1. Voltages induced in any two windings due to changes in mutual flux will have the <u>same</u> polarity at "dot-marked" terminals.

RULE 2. If positive currents flow into the "dot-marked" terminals of related windings, then the mmf's produced in each winding will have additive polarity.





- - RELATIVE TO WINDING A-B
- ▲ RELATIVE TO WINDING E-F
- - RELATIVE TO WINDING C-D

Figure 2 Determining flux directions (a), and dotting of windings (b).

RULE 3. If any related winding is open-circuited, and if the currents flowing into the "dot-marked" terminals have a positive rate of change, then the voltage induced in the open winding will be positive at its "dot-marked" terminal.

When a magnetic circuit arrangement has more than two windings and contains more than one major flux path, then multiple "dotting" windings is necessary to visually express voltage polarities. However, this is easily done by the use of the right hand rule and the three dotting rules given above. An example of multiple "dotting" is shown in Figure 2(b), where three sets of "dots" are needed to express winding polarities relative to each one of the three windings of the magnetic.

2.1 A Magnetic Circuit Modeling Example

All of the fundamental definitions related to magnetic circuits given above, when combined with the techniques of electric circuit modeling and duality, produce a powerful set of analysis tools for quick and accurate examination of any magnetic circuit arrangement, no matter how complex it may be. The electric circuit models that result are just that - circuit models - and do not depend on abstract mathematical relationships (such as mutual inductance expressions) for performance evaluations.

As an illustration of the power of these modeling techniques, consider now an example. For this exercise, we will derive an electric circuit model for a two-winding transformer with parasitic leakage inductances, as shown in Figure 3(a). Here, an ungapped toroidal core provides the major magnetic path between windings (\emptyset_m) , and each winding has a leakage path $(\emptyset_1,\ \emptyset_2)$ for flux that is not contained in the material path. We will assume for this exercise that the core's cross-sectional area is uniform throughout its body, and that a mean path length can be used to define the reluctance of the core.

If we designate N_p as the primary exciting winding, we can first determine the voltage polarity of the secondary winding using the right-hand rule. With a primary current direction and the winding dotted as shown in Figure 3(a), fluxes \emptyset_1 , and \emptyset_2 must have positive directions as indicated in this figure. The dot for the secondary therefore must be at the top of this winding to produce a flux in the same direction as \emptyset_m .

With winding polarities established, we note that the secondary voltage, v_0 , must have a polarity as shown, for the given polarity of exciting voltage, v_s . Because the resulting secondary current is "out of the dot", we also note from our earlier transformer rules that this current, i_0 , will produce an mmf that opposes that of the primary.

Next, we draw the equivalent magnetic circuit diagram for the arrangement of Figure 3(a). This is done in Figure 3(b), using the analogous relationships defined earlier. Note that \mathscr{G}_m and \mathscr{G}_1 have the same polarity in the primary winding, since they are caused by isomower, in the secondary winding, \mathscr{G}_m and \mathscr{G}_2 have opposite polarity, since one flux (\mathscr{G}_m) produces io while the other (\mathscr{G}_2) is a consequence of io

From the magnetic circuit of Figure 3(b), we can now develop a dual permeance network for it, resulting in the equivalent circuit of Figure 3(c). Our next step is to scale the network of Figure 3(c) by the number of turns of the winding we select as reference for the final electric circuit representation. This is accomplished in Figure 3(d). The major purpose of this scaling step is to place all circuit permances in a form that can be directly related to inductance. Note that the scaled model of Figure 3(d) also permits easy conversion of flux linkages to primary and secondary voltage values.

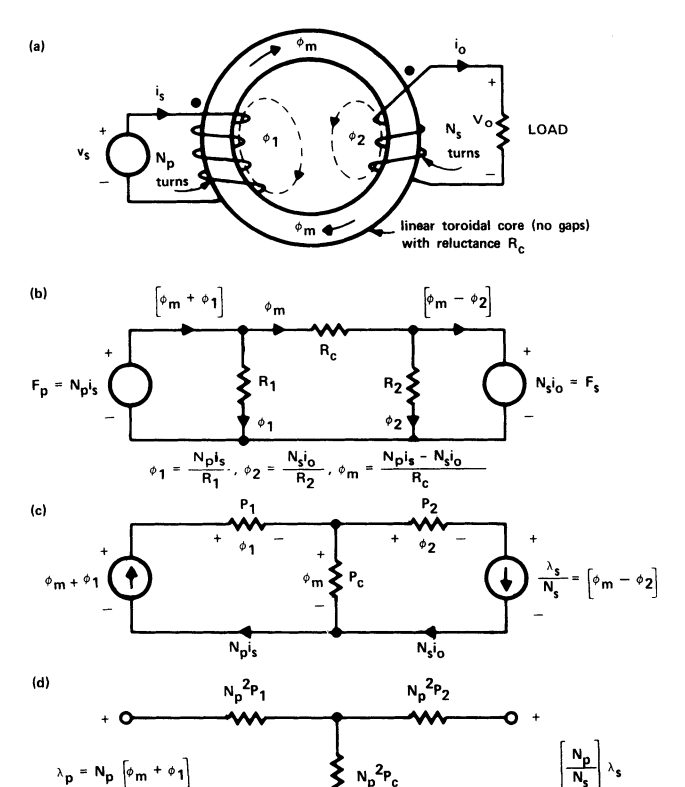


Figure 3 Developing reluctance and permeance circuit models for a two-winding transformer with leakage fluxes.

Finally, we convert the scaled permeance network to one involving voltages and inductances. This conversion is shown in Figure 4(a). Note that we have added an ideal transformer to this network to properly scale terminal secondary voltage and current values. Using impedance translation methods, we can also "move" all or some primary inductances to the secondary side of the final electric circuit model if desired. Two versions of such impedance movements are shown in Figures 4(b) and 4(c).

In just four easy steps, we have been able to develop a realistic electric circuit model for a somewhat complex magnetic circuit arrangement. Note that the final models of Figure 4 do not involve mutual inductances and are in a form that a designer can easily relate physical properties of the corresponding magnetic system of Figure 3(a) to familiar electric circuit quantities.

Looking at Figure 4(c), we see that inductances $\rm L_1$ and $\rm L_2$ represent those

produced by flux leakages, and are often called leakage inductances. Inductance L_C in the networks of Figure 4 represents that produced by the primary turns $\left(N_{D}\right)$ wound on the ferromagnetic core of the transformer, and is not the mutual inductance (M) shared by primary and secondary windings. Recall that mutual inductance is a mathematical measure of the degree of coupling between two windings of a magnetic. In this case, we can easily find the value of M by writing the two nodal equations that relate input and output currents of the circuit models, and then isolate the common inductance terms within them. If this is done, then M is found to be:

$$M = \frac{NS}{Np} \cdot L_C \tag{6}$$

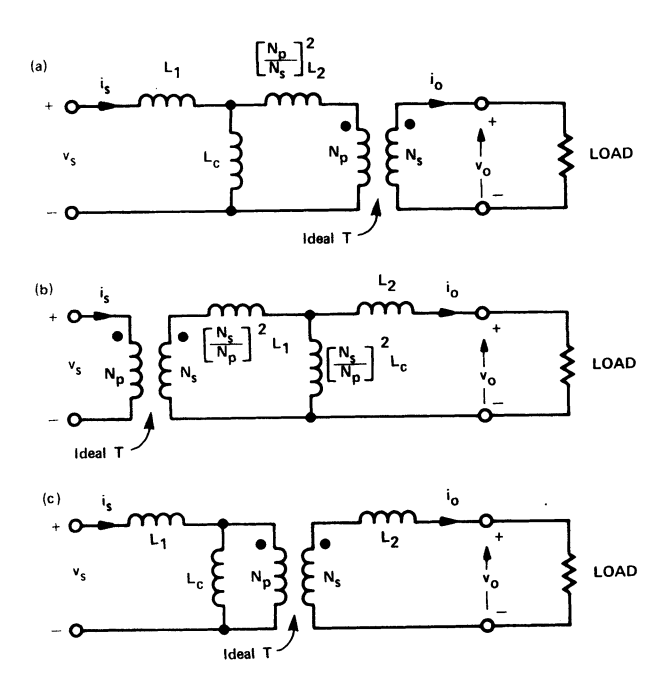


Figure 4 Electric-circuit equivalent networks for the two-winding transformer of Figure 3(a).

3 ACHIEVING ZERO RIPPLE CURRENTS

Although the techniques of achieving zero ripple currents in the windings of selected magnetic designs have recently been thoroughly explored [10], there is much historical evidence that the use of magnetic means to lower ripple currents in converter outputs is not a new discovery. For example, G.B. Crouse disclosed in his 1933 United States patent [6] a magnetic method for lowering

the ripple voltage of an L-C filter for use in radio receiver power supplies. This method, upon close scrutiny, appears to be identical to one reported some years later by S. Feng [7] for reducing the size of filter capacitors used across the outputs of power converters.

In both cases, the method entailed the addition of another winding to the filter inductor, whose mutual inductance relationship to the original inductor winding was selected by design to "steer" the ripple current in the main winding to the added "secondary" winding and, therefore, away from the output of the filter. The resulting circuit arrangement is shown schematically in Figure 5, for application as the secondary filter of a forward converter. Note that a filter capacitor (C) is necessary for DC isolation of the "inter" winding and is selected to maintain an average voltage across it equal to V_0 in the presence of the ripple current. Ideally, the mutual inductance shared by the inductor windings is then chosen to completely remove the ripple current from the load (R) and to steer it to the inner winding (N_3) . For this reason, no output filter capacitor is shown across R in Figure 5. However, in practical designs, some capacitance is usually added across R for decoupling of noise and for additional energy storage for instantaneous load demands.

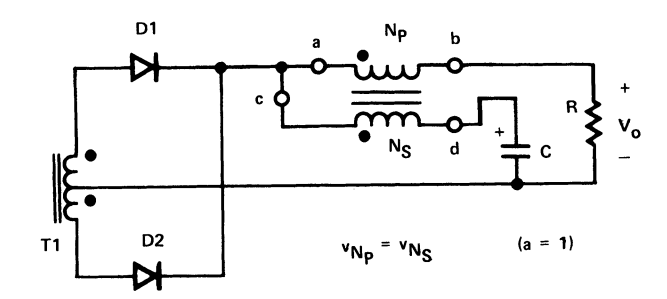


Figure 5 "Coupled-Inductor" output filter network of a quasi-squarewave converter.

To understand how the inductor arrangement of Figure 5 can magnetically reduce ripple currents, we can use the electric circuit model developed in Section 2.1. Looking at Figure 5, we can assume that the voltages impressed across the two windings of the inductor are proportional in amplitude and equal in dynamic periods, such as those shown in Figure 6(a). For our purposes, we will therefore assume that the "primary" voltage is of a value equal to v_s, with the "secondary" excited by another proportional voltage, av_s. With these

assumptions, we can impose these voltages across the terminals of the electric circuit model form Figure 4(c), and then analyze what model values must be present to make the primary ripple current (i $_{\rm S}$) vanish.

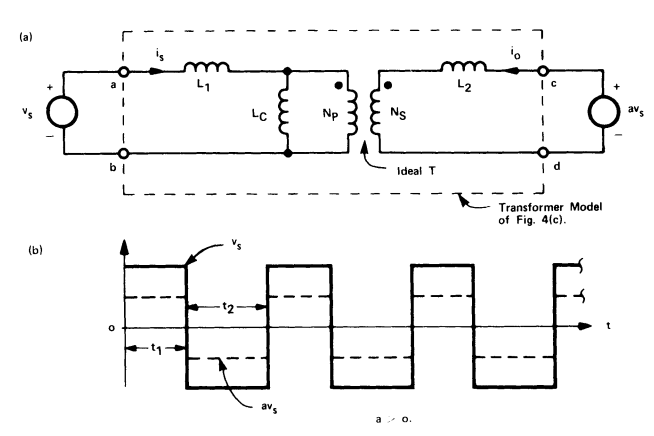


Figure 6 The coupled-inductor of Figure 5 modeled using the transformer equivalent circuit (a), driven by proportional voltages (b). (Note: a = 1 for Figure 5).

This analysis task is easily performed, as illustrated in Figure 7. Writing the circuit equations for Figure 7(b) gives:

$$av_{s} = \left[L_{2} + \left(\frac{N_{S}}{N_{P}}\right)^{2} L_{C}\right] \frac{dio}{dt}$$
 (7)

$$\left(\frac{N_{S}}{N_{P}}\right)v_{S} = \left(\frac{N_{S}}{N_{P}}\right)^{2} L_{c}\left(\frac{dio}{dt}\right)$$
(8)

$$L_2^{\cdot} = \left(\frac{N_S}{N_p}\right)^2 L_c \left[\frac{aNp}{N_S} - 1\right]$$
 (9)

Therefore, if we select the leakage inductance of the secondary winding to meet the needs of (9), then the primary ripple current will be reduced to zero! Although not shown here, a similar analysis of the circuit model of Figure 6(b) for zero-ripple secondary current can be made. The value of primary leakage inductance for i_0 = 0 is then found to be:

$$L_1 = L_c \left(\frac{N_S}{aN_P} - 1 \right) \tag{10}$$

Comparing the constraints imposed on the values of L_2 and L_1 by (9) and (10), respectively, one finds that it is not possible to achieve zero values of i_s and i_0 simultaneously. This point is also made by the current waveforms for i_s and

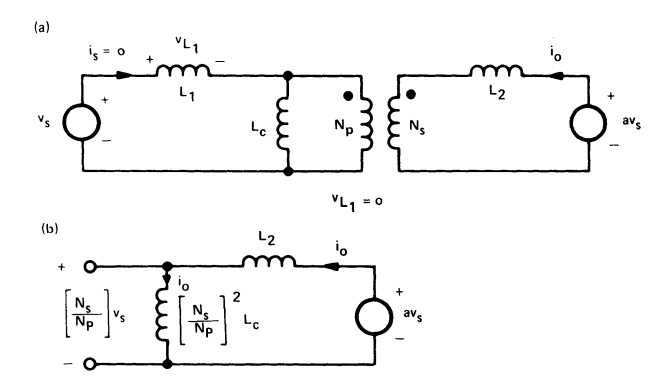


Figure 7 Circuit conditions in the model of Figure 6 for $i_c = 0$.

 i_0 illustrated in Figure 8. Note also from the equations accompanying Figure 8 that the **effective** inductance seen at the "primary" terminals of the two-winding magnetic will be equal to its opencircuit value (i.e. "secondary" side open) when L_1 is selected to reduce i_0 to zero. Conversely, the effective inductance seen at the "secondary" terminals will be equal to its opencircuit magnitude when L_2 is set to reduce i_8 to zero.

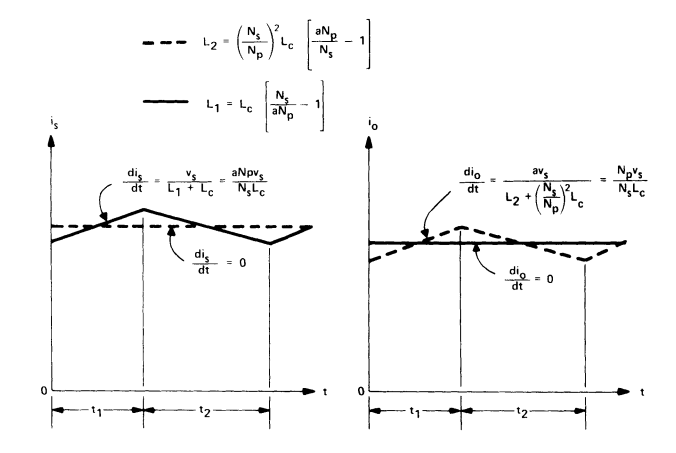


Figure 8 Input and output current waveforms of Figure 6(a) when selected values of L_1 or L_2 are present (Note: a = 1 for Figure 6(a)).

In actual practice, it is difficult to design and manufacture magnetic assemblies with consistent and specific values of parasitic leakage inductances to achieve the zero-ripple current conditions as defined by (9) or (10). One viable solution to this producibility problem is to tightly wind primary and secondary turns to reduce L_1 and L_2 to essentially zero, and then to insert a small external "trimming" inductor [8] in

series with the input or output to emulate the required inductance needed for L_1 or L_2 . This trimming method is shown in Figure 9, along with corresponding values of L_{ext} necessary for zero-ripple current conditions.

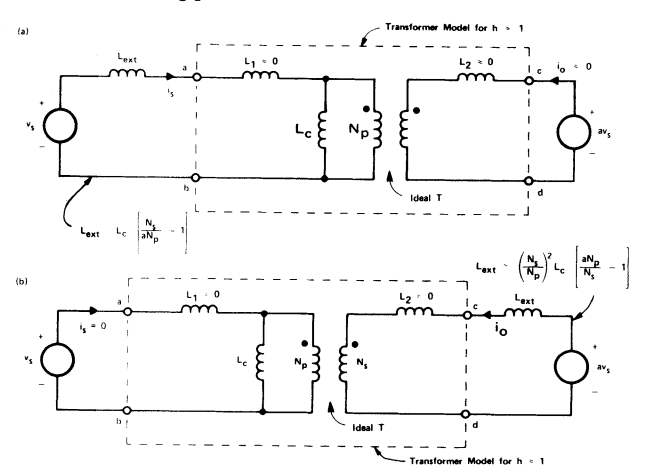


Figure 9 Using small external inductances to trim ripple current magnitudes in the circuit of Figure 6(a).

Because of recent emphasis on application of zero-ripple-current filters in 'Cuk converter variations [9], [10], it is now generally believed that this particular family of converter topologies is the only one that can benefit by their use. However, as we have just seen, this is not the case. In boost converters, these same principles of ripple current reduction can be applied to their input inductor arrangements, one example of which is shown in Figure 10. And, as we will soon see, this method of ripple current reduction can also be advantageously used in both buck and boost derived integrated-magnetic converter systems.

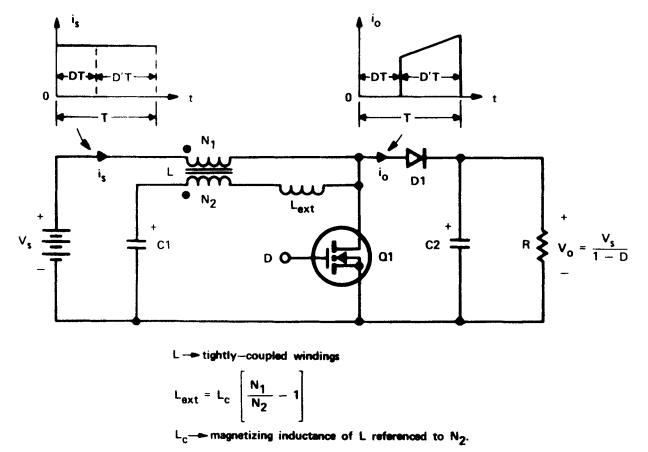


Figure 10 Using a coupled-inductor arrangement in a basic boost converter to reduce input ripple current magnitude.

4 DEVELOPING AN INTEGRATED-MAGNETIC FORWARD CONVERTER

It is interesting to note that, contrary to popular belief [3], integratedmagnetic concepts for power converters are not innovations of research performed over the past seven years. Like the magnetic methods of ripple current reduction described in the last section of this paper, the concept of integration of the magnetic functions of power processing circuits has historical roots in much earlier periods. Perhaps the best documented evidence of this fact is an obscure (and mis-titled) United States patent by Cielo and Hoffman of the IBM Corporation [11]in 1971, which discloses possible circuit methods for integration of the transformer and inductor of so-called "push-pull" DC-to-DC converters. Later in this paper, we will examine the methods of this interesting patent by extending the integrated-magnetic forward converter concepts to include "push-pull" switch arrangements.

With a brief exposure to magnetic circuit modeling methods and a review of inductive ripple current reduction techniques behind us, let us proceed to systematically construct a **single** magnetic assembly wherein the transformer and the inductor of a forward converter can be contained. No rigorous synthesis procedure will be followed here, but rather a path of **deduction and intuition** based on the general operation of this converter and knowledge of the flux change relationships that must exist in its inductive components.

The first step in our integration process will be to redraw the forward converter circuit of Figure 1 in a manner so as to emphasize both the electrical and magnetic aspects of the converter. assuming that the converter is operating in the continuous mode of inductor energy storage, the equations describing circuit conditions for each of the two switching states are found, and then placed in a format relating corresponding flux changes in the transformer and inductor. Because we are interested at this time in only major flux relationships, the describing circuit equations can be ideal, thus ignoring all parasitics including switch and diode drops, switching losses, etc. The elimination of parasitics is not a requirement, but it is a convenience for this discussion.

The redrawn forward converter is illustrated in Figure 11. The core of the transformer is shown ungapped, while the inductor core is shown with an air gap, as is the usual case for a magnetic that must withstand DC bias. Transformer

windings are drawn and dotted to emphasize an assumed counter-clockwise direction of flux in its core and to produce a positive voltage (v_1) across the secondary winding (N_S) when the primary switch (Q1) is ON. Note also that we have included a "core-reset" winding (N_{p2}) on the transformer for energy removal during intervals when Q1 is OFF. A core material with low residual flux is presumed. For the inductor with its winding position as shown, flux direction will be clockwise.

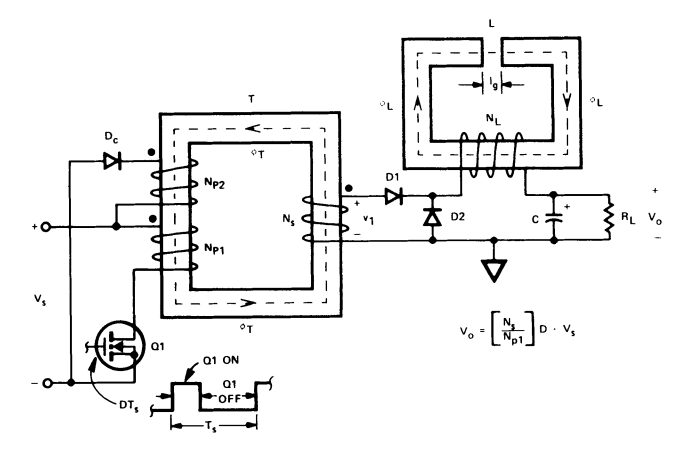


Figure 11 Conventional forward DC-DC power converter (idealized) drawn to emphasize magnetic operations.

Next, the ideal voltages that appear across the transformer and inductor windings are found by simple circuit analysis for each of the two switching states of the converter, DT_{S} and $(1\text{-D})\text{T}_{\text{S}}$ = D'Ts. Using (1), we then relate the rate of flux change in the transformer core (\emptyset_{T}) and in the inductor (\emptyset_{L}) to these voltage magnitudes.

DURING DT:

$$\dot{\mathbf{g}}_{T} = \frac{d\mathbf{g}_{T}}{dt} = \frac{V_{S}}{N_{P1}} = \frac{V_{1}}{N_{S}}$$
 (11)

$$\dot{\mathbf{p}}_{L} = \frac{d\mathbf{p}_{L}}{dt} = \frac{V_{1}}{N_{L}} - \frac{V_{0}}{N_{L}}$$
 (12)

DURING D'T:

$$\dot{\mathbf{g}}_{T} = \frac{V_{S}}{N_{P2}} \tag{13}$$

$$\dot{\mathbf{g}}_{L} = \frac{V_{O}}{N_{I}} \tag{14}$$

Looking at the equations for interval $_{\mbox{DT}_{\mbox{S}}},$ we see that we can combine them to remove the intermediate secondary voltage

value, V1:

$$\dot{\boldsymbol{\beta}}_{T} = \left(\frac{N_{L}}{N_{S}}\right) \boldsymbol{\beta}_{L} + \frac{V_{O}}{N_{S}}$$
(15)

Note that the last term of (15) is of a form that could be considered as defining a flux change in a magnetic medium that is **dependent** on the value of the output voltage, V_0 , of the converter and the number of secondary turns on the transformer, N_s . It follows then, that if we make this consideration, that such a magnetic medium must be a part of the transformer assembly to satisfy the conditions of (15). Therefore, we can rewrite (15) as:

$$\dot{\boldsymbol{\beta}}_{T} = \left(\frac{N_{L}}{N_{S}}\right)\dot{\boldsymbol{\beta}}_{L} + \dot{\boldsymbol{\beta}}_{O} \tag{16}$$

where $\dot{0}_0 = V_0/N_s$. Turning now to the first right-hand term of (15) and (16), we note that its contribution to ${\it G}_T$ is dependent on a fraction, N_L/N_S , of the flux change rate in the inductor of the Since our ultimate goal is converter. to make the inductor an integral part of the same magnetic assembly that also contains the transformer windings, it is logical to assume that $\rm N_L$ should be made equal to $\rm N_S$, so as to contain all inductor flux in a single magnetic path. As we will see later when we analyze the integrated magnetic that results from this "synthesis" exercise, N_s must be equal to $N_{
m L}$ to realize a non-pulsating output current waveform and to achieve an input-to-output voltage transfer function that matches that of a forward converter.

Setting $N_L = N_S$ in (16), we arrive at a final expression for g_T during interval DT_S :

$$\dot{\boldsymbol{g}}_{\mathsf{T}} = \dot{\boldsymbol{g}}_{\mathsf{L}} + \dot{\boldsymbol{g}}_{\mathsf{O}} \tag{17}$$

Remembering our previous magnetic modeling, we can interpret (17) as defining a magnetic assembly in which there are three major flux paths. This equation also tells us that the flux change in an input source related path $(\mathring{\theta}_T)$ contributes to the change in another path $(\mathring{\theta}_L)$ associated with the "inductor" portion of the assembly, as well as to flux change $(\mathring{\theta}_0)$ in a third path. From the assumption made in (16), this third path is related to the output voltage value of the converter.

These general observations permit us now to sketch a possible magnetic path arrangement that satisfies the conditions of (17) for the switching interval DTs. This sketch is shown in Figure 12(a). Note that the "inductor" path includes an airgap, as we expect that this leg of the magnetic core will need one to establish the required amount of storage inductance and to sustain DC bias without material saturation. To the outer legs of the core arrangement, we have added windings for primary and secondary in accord with (11) and (12), dotted properly to produce the required polarity of $\rm V_0$ for the indicated directions of $\rm i_s$ and $\rm i_0$.

Using the magnetic arrangement of Figure 12(a) as a baseline, we now look at what must be added to permit the conditions of (13) and (14) to be satisfied for the other switching interval D'Ts. First, a winding to release the energy stored in the center leg is needed, and its turns (N_L) must equal those of N_S from our earlier discussions. Second, a winding (N_{P2}) is needed in the same leg of the core as that of the primary for "reset" purposes. The magnetic arrangement that results is shown in Figure 12(b). Note that these two windings are dotted so as to produce the **same** flux directions in their respective core legs as those in Figure 12(a).

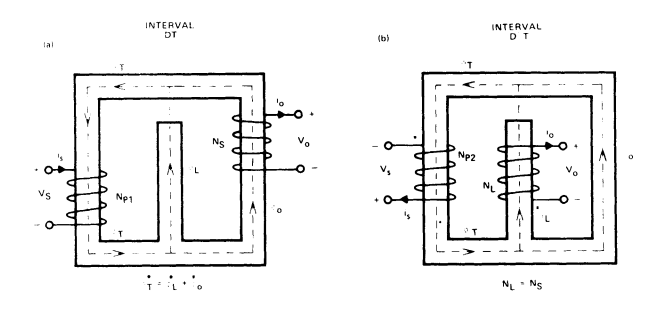


Figure 12 Developing magnetic core arrangements for each state of the converter in Figure 11.

Our final task in this deductive "synthesis" process is to combine the two magnetic arrangements of figure 12 by the addition of switches and diodes to establish the required winding voltage values for each switching interval of the converter. From our knowledge of the forward converter, we would expect that no more than one switch and two diodes would be needed, and this is indeed the case.

Figure 13 is the schematic of the integrated-magnetic version of the

forward converter that results from our efforts. Reflecting now on the steps that were necessary to place the transformer and inductor on a single-core structure, we find that no exotic efforts were really required and that, in reality, the deductive procedure followed was rather straight-forward and elegantly simplistic. It now becomes clear that we can use similar deductive methods to evolve integrated-magnetic versions of any transformer-isolated buck-derived converter. Once this is done, we can then use the principles of duality between converter circuits [12], [13] to formulate complimentary boost topologies.

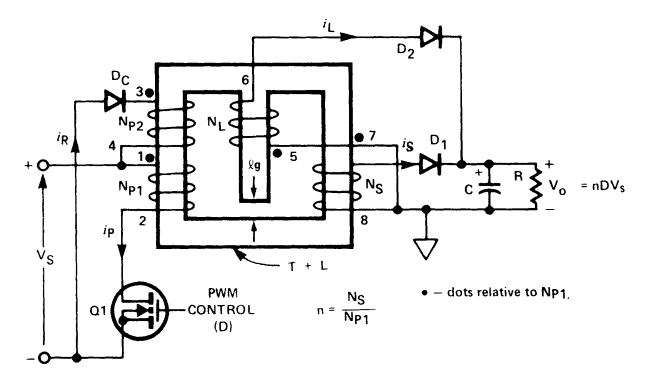


Figure 13 A forward converter with integrated magnetics.

4.1 Verification By Analysis

Following the evolution of an integrated magnetic arrangement for a converter, it is worthwhile, if not mandatory, that its structure by verified by analysis. This is necessary in order that no major design aspect has been overlooked, as well as to examine the effects of any circuit parasitics (such as leakage inductances, etc.) that may have been introduced by the integration process.

For the integrated-magnetic forward design of Figure 13, the analysis procedure begins with the extraction of the magnetic from the overall circuit topology, labeling each winding as to voltage polarities as well as current directions that are imposed by the converter. It is also advantageous to mark each winding terminal and carry the identifying marks through the modeling procedure, so that the final electric circuit model found by the analysis can be directly substituted for the magnetic assembly in the converter topology.

An isometric sketch of the extracted magnetic from Figure 13 is shown in Figure 14(a). To this sketch, we add flux directions in each leg, assuming

that the primary winding, Npl, is the exciting and dominant winding of the magnetic. From this point on, the analysis procedure follows the same steps of the two-winding transformer example of Section 2.1, keeping in mind that there are three magnetic paths and four sources of mmf in this case. Also, since we are only interested in major flux paths, we have omitted all leakages for this examination. However, they can be easily added later and the corresponding electric circuit model changed to reflect their presence.

- UNIFORM CROSS-SECTIONAL AREA (A_C) THROUGHOUT
- MATERIAL PERMEABILITY OF ALL SECTIONS IS THE GAME
- DOTS RELATIVE TO N_{P1}

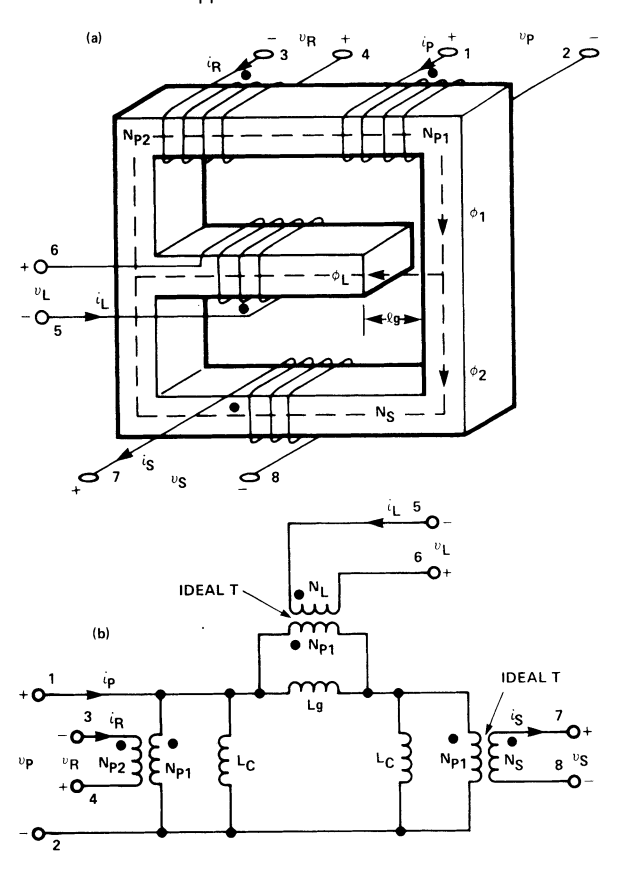


Figure 14 An electric model (b) for the magnetic system of (a) taken from Figure 13.

The electric circuit model of the magnetic of Figure 14(a) is shown in Figure 14(b). For the sake of brevity, we have not included the intermediate steps of the modeling effort here, but they can be found in [14]. This particular model is referenced to the main primary of the magnetic, Np1, as evidenced by the turns ratios of the

three ideal transformers within it. Inductance Lg represents that presented by the center-leg winding, while the two inductances, $L_{\rm C}$, represent those presented by the outer-leg windings of the core (Referenced to $N_{\rm Pl}$).

The next step is to place the elctric circuit model into the converter circuit, as shown in Figure 15. In making this placement, we have also "moved" Lg and one of the two $L_{_{\hbox{\scriptsize C}}}$ inductances "through" the ideal transformer of turns ratio Npj: $N_{\rm S}$, using standard impedance translation This is done to position most methods. of the inductances to the "right" of this transformer in order that the final equivalent converter circuit can be compared to that of a forward converter with discrete magnetics. Note that this impedance movement also required a change in the turns ratio of the ideal transformer across Lg.

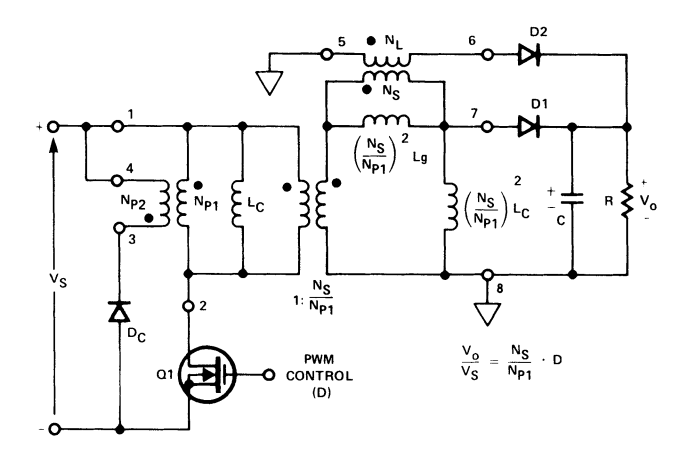


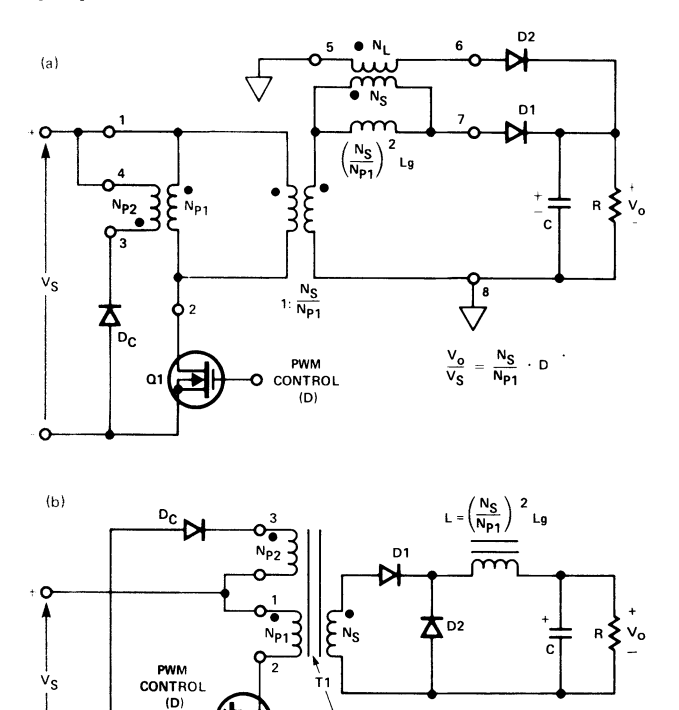
Figure 15 Placing the model of Figure 14(b) into the topology of Figure 13.

In practical designs, we would expect that L_C would be much larger in inductance value than Lg, since the permeability of free air is much less than that of a ferromagnetic material. Therefore, we can simplify our analysis at this point by eliminating the reflected L_C across terminals 7 and 8 of the circuit model in Figure 15. Also, we can assume that the L_C across terminals 1 and 2 of the model can be viewed as the "magnetizing inductance" of a real transformer of ratio N_{P1}: N_S. It is also apparent that winding N_{P2} can be a part of this same transformer, since it parallels L_C.

With these assumptions in mind, we can now redraw the circuit of Figure 15 in a slightly simpler form shown in Figure 16(a). We also remember that the

integrated converter of Figure 13 also constrained $\rm N_L$ to be equal to $\rm N_S$ and, therefore, the turns ratio of the ideal transformer across L has been changed accordingly in Figure 16(a). With the turns ratio of this transformer now 1:1, it can be completely removed by simply re-orientating the circuit positions of diodes D1 and D2.

This final analysis step leads to the converter configuration of Figure 16(b), which matches that of a conventional forward converter! We see also that the equivalent output inductance of this converter is equal to that set by the gap of the integrated-magnetic multiplied by the squared ratio of "transformer" secondary-to-primary turns. If we had not chosen N_{L} to be equal to $\text{N}_{\text{S}}\text{,}$ this equivalent circuit and its predecessor in Figure 16(a) tells us that the equivalent inductance would not be of the same value for each switching state of the converter and, therefore, we could expect the output current to be somewhat pulsating, just as would be experienced in a forward converter with a "tapped" output inductor [14]!



(MAGNETIZING INDUCTANCE = LC)

N_{P1} , N_{P2} → TIGHTLY COUPLED

Figure 16 Further circuit manipulation (a) to derive the discrete magnetic version of Figure 13 shown in (b).

It is evident from the results obtained above, that the analysis of an integrated magnetic by the use of electric model equivalents has great value and provides much valuable design information. particularly valuable in designing integrated-magnetic versions of existing converter designs, where filter inductances and transformer characteristics (turns ratios, etc.) are known quantities. Using the equivalent circuit, such as the one in Figure 16(b), these quantities can then be directly related to the parameters of the integrated magnetic, such as core dimensions and permeabilities, winding turns, etc.

4.3 Voltage and Current Waveforms

From a "black box" standpoint, we would expect an integrated-magnetic version of a converter to have the same voltage and current characteristics as its discrete-magnetic counterpart. For the forward converter design of Figure 13, this is indeed the case, as is evidenced by the dynamic current and voltage waveforms of Figures 17 and 18, respectively. These

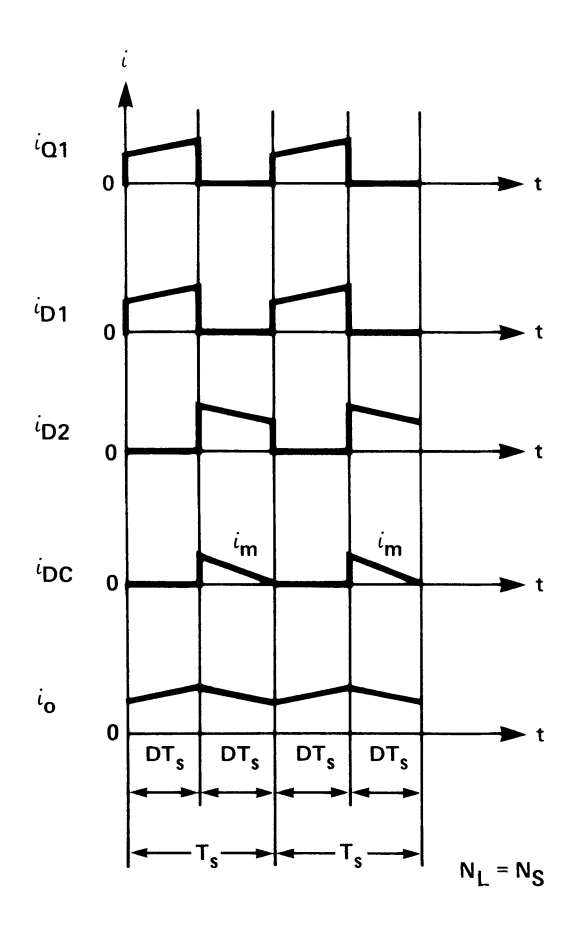


Figure 17 Idealized currents in the SPC topology of Figure 13 (continuous mode).

waveforms and their magnitudes were derived by inspection of the current and voltage conditions that must exist in the electrical circuit models of Figures 15 and 16 for each converter state (continuous mode of energy storage assumed). As we see from both sets of waveforms, current and voltage stresses on the switches and diodes remain the same as those that would be experienced in a conventional forward design.

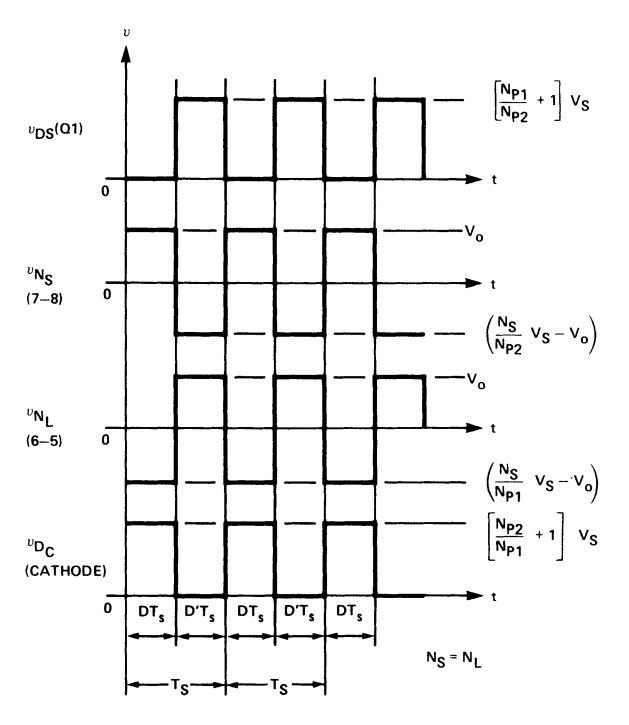


Figure 18 Voltage waveforms in the SPC of Figure 13 (continuous mode).

5 DEVELOPING INTEGRATED-MAGNETIC BOOST CONVERTERS

It is possible to follow similar procedures of deductive synthesis and analysis from the last section of this paper to evolve integrated-magnetic versions of various boost-derived converters, such as the reverse converter [13] in Figure 1. However, given a dual buck-derived converter approach, it is much easier to use duality methods [12], [13] to derive these complimentary circuits.

For example, given the integrated-magnetic forward converter, duality manipulations then produce the integrated-magnetic boost equivalent of the reverse converter of Figure 1. The unusual converter that results is shown in Figure 19. In this case, when Q2 is ON, energy is stored in the center-leg of the magnetic. During this same time

period $(\mathrm{DT_S})$, load needs are supported by the output capacitor, C, and by magnetizing energy stored in the outer leg of the magnetic from the previous switching cycle (via D3). When Q2 turns OFF, Q1 is turned ON and the energy stored in the center leg is magnetically routed to the output load, R, via winding $\mathrm{N_S}$, with diode D1 now forward-biased and the other diodes non-conducting. Like its discrete-magnetic contemprary in Figure 1, the ideal input-to-output voltage transfer function is simply:

$$\frac{V_0}{V_S} = \frac{N_S}{N_P} \cdot \frac{1}{1 - D} \tag{18}$$

with the "inductor" turns equal to that of the "primary" winding of the magnetic assembly.

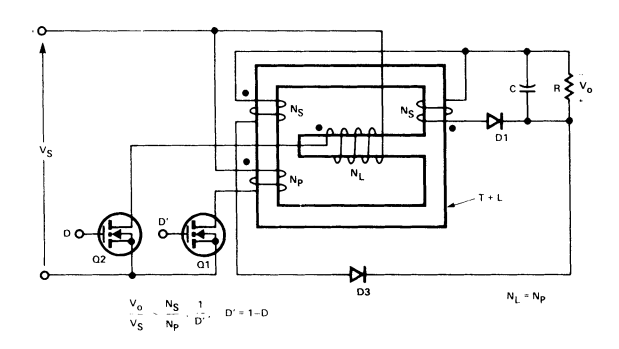


Figure 19 An integrated-magnetic version of the reverse converter shown in Figure 1.

6 ADDING ZERO-RIPPLE CURRENT FEATURES

Magnetic integration of the inductors and the tranformers of buck and boost-derived converters does <u>not</u> lessen the possibility of adding additional windings to control ripple current magnitudes on output or input lines.

As we have seen in prior examples of integrated-magnetic forward and reverse converters, the inductive part of their magnetic assemblies is isolated to one path of the core arrangement. Therefore, by adding another winding in these same paths and impressing a voltage across it that is proportional in amplitude and of the same frequency as that appearing across the original inductor winding, we can steer the ripple current from the inductor winding to the other winding and, therefore, away from the output. also have the option of "trimming" the ripple current magnitude by external means [8] if we so desire.

Figure 20 shows an integrated-magnetic forward converter with output ripple current control capability. Note that another winding has been added to the center-leg section (N_{LR}), along with a small series inductor (L_{χ}) and DC-isolation capacitor (C_{R}). Winding N_{L} is the original inductor winding and the new winding, N_{LR} , is wound in close proximity with it. This is done to minimize leakage inductance effects and to maximize the mutual inductance that will exist between the two windings.

With the new winding positioned in the converter circuit as shown in Figure 20, the value of inductance L_{χ} needed to cause the output ripple current to vanish is found easily using (9) with a = 1:

$$L_{\chi} = \left(\frac{N_{LR}}{N_{L}}\right)^{2} L_{g}\left(\frac{N_{L}}{N_{LR}} - 1\right)$$
 (19)

where Lg is the inductance presented by the airgap of the center leg with ${\tt N}_{L}$ turns.

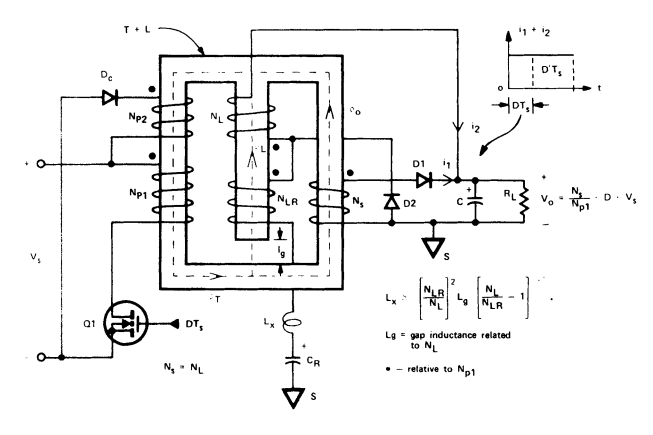


Figure 20 Adding ripple control features to the integrated-magnetic forward converter of Figure 13. (N_{\parallel} , N_{\parallel} , tightly coupled).

In a similar manner, a ripple-control winding can be added to the integrated magnetic of a reverse converter, as is done in Figure 21. In this case, the value of L_X to reduce the input ripple current to zero is again the same as given by the solution of (19), assuming that windings N_L and N_{LR} are tightly coupled together.

In actual designs, there will be some slight slope in the "zero" ripple currents of these two converters due to the presence of the inductances ($L_{\rm C}$) of the outer-leg primary and secondary

windings. However, since $L_{\rm C}$ is usually much greater in value than that posed by the "inductor" winding, Lg, this deviation from an ideally flat current waveform is normally so small that it can be neglected for all practical purposes.

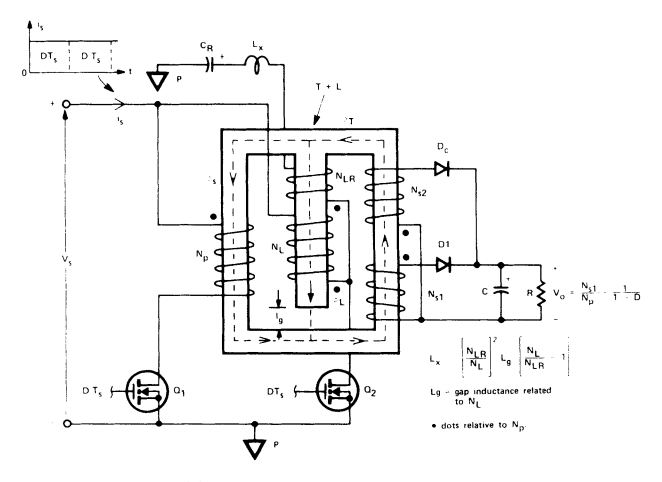


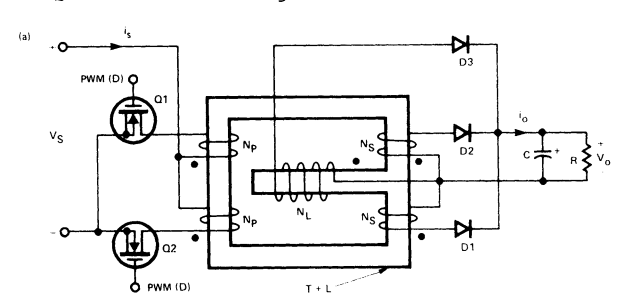
Figure 21 Adding ripple control features to the integrated-magnetic reverse converter of Figure 19. (N_L, N_{LR} tightly coupled).

7 PUSH-PULL DESIGNS WITH INTEGRATED MAGNETICS

Just as there are so-called "push-pull" versions of the forward converter with discrete magnetics, integrated-magnetic arrangements are also possible. Two viable approaches [11] are shown in Figure 22. The first alternative, shown in part (a) of this illustration, looks very similar to the single-switch forward design of Figure 13, except that another set of primary and secondary windings have been added on opposing sides of the outer portion of the core structure. With the windings dotted as shown (relative to the primary winding, $N_{\rm p},$ controlled by Q1), diode D1 will conduct when Ql is ON, and diode D2 will conduct when Q2 is ON. During both conduction intervals, energy is stored in the center leg of the magnetic, and is then released to the load via diode D3 when Q1 and Q2 are both OFF.

In the case of the second alternative shown in Figure 22(b), note that the phasing relationships (i.e. dots) of the two secondary windings (N_S) have been changed from those of Figure 22(a). This change now prevents significant energy from being stored in the center leg of the magnetic, since conducting secondaries lie on the same magnetic path as their corresponding primary windings. For example, in Figure 22(b), when Ql is

ON, D1 will conduct and when Q2 is ON, D2 conducts. Therefore, another winding (N_{L1}) has been added to the center leg to provide a means of energy storage in the center leg when either Q1 or Q2 is conducting.



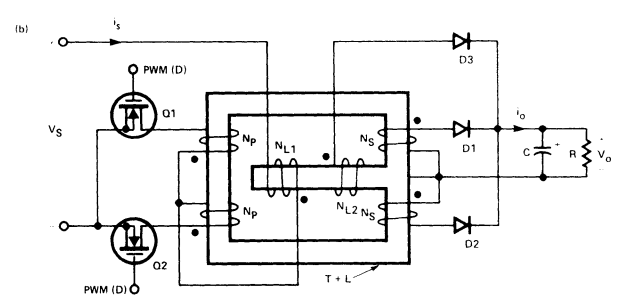


Figure 22 Two "push-pull" versions of the forward converter of Figure 13.

7.1 Ideal Voltage Transfer Functions

The input-to-output voltage relationships for the continuous mode of inductive energy storage for the converters of Figure 22 can be easily found by equating the volt-seconds appearing in the center leg of their integrated-magnetic assemblies during each of the two switching intervals, DT_S and D'T_S. In the case of Figure 22(a), the DC voltage transfer is ideally found to be:

$$\frac{V_{0}}{V_{S}} = \frac{N_{L}}{N_{S}} \left\{ \frac{D}{1 - D(1 - (N_{L}/N_{S}))} \right\}$$
 (20)

For N_s equal to N_L , (20) reduces to:

$$\frac{V_0}{V_S} = \frac{N_S}{N_P} \cdot D \tag{21}$$

which confirms that this integratedmagnetic converter design is buckderived. For the other circuit arrangement in Figure 22(b), the DC voltage transfer function is ideally:

$$\frac{V_{Q}}{V_{S}} = \frac{N_{S}}{N_{P}} \left[\frac{1}{1 + (D'/D)(N_{L1}/N_{L2})(N_{S}/N_{P})} \right]$$
(22)

In this instance, if:

$$\frac{N_{P}}{N_{S}} = \frac{N_{L1}}{N_{L2}} \tag{23}$$

then (22) becomes:

$$\frac{V_O}{V_S} = \frac{N_S}{N_P} \cdot D \tag{24}$$

which, like (21), confirms that this circuit variation is a member of the buck derived converter family. Interestingly enough, this converter, with its magnetic replaced by its electric-circuit equivalent [14], is found to be an integrated-magnetic version of the Weinberg circuit [15]!

7.2 Voltage and Current Waveforms

The typical current and voltage waveforms that will be observed in either converter circuit of Figure 22 are shown in Figures 23 and 24, respectively. In the case of the current waveforms, they look very similar to those of a conventional "pushpull" quasi-squarewave converter, except that the magnetizing current of the outer legs of the magnetic produces a minor step in the otherwise continuous form of the output current. As discussed earlier, these "steps" will usually be very small because of the high values of effective inductances of the windings on the outer legs.

Voltage waveforms also are quite similar to those of a "push-pull" buck-derived converter, except that the magnetic integration process has yielded another potential benefit - lower OFF voltage stress on the two switches of the converter. Ideally, the OFF voltage stress on either switch in a conventional "push-pull" converter will be equal to a maximum value of twice the input voltage magnitude. However, in its integratedmagnetic version (Figure 22(a), maximum OFF voltage stress is equal to the value of source voltage plus the reflected output voltage. This implies that, by proper choice of turns ratio, we can significantly reduce switch voltage stress by using integrated magnetics as compared to a conventional discretemagnetic equivalent!

7.3 Practical Design considerations

In order to reduce the possible harmful effects of leakage inductances, the integrated-magnetic circuit variation of Figure 22(b) is often preferred over that

of its contemporary approach in Figure 22(a). Note that, in Figure 22(a), corresponding primaries and secondaries are positioned on the core legs so that they cannot be tightly coupled together (i.e. wound tightly together). However, in the converter of Figure 22(b), because corresponding primaries and secondaries lie on the same legs of the core structure, they can be wound tightly together to maximize their magnetic coupling and to minimize parasitic leakage inductances. Therefore, for this reason, the design of Figure 22(b) is usually chosen rather than the circuit of Figure 22(a), even though the latter approach requires an additional winding to be added to the center leg for energy storage.

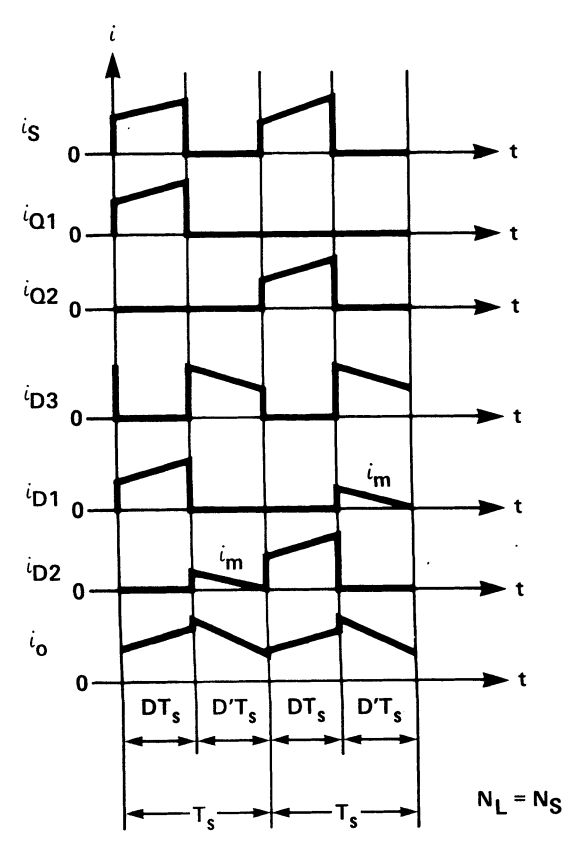


Figure 23 Ideal current waveforms in the converters of Figure 22 (continuous mode).

Another advantage of the converter in Figure 22(b) is the presence of an inductor in series with both primary switches. Thus, high instantaneous current due to conduction time overlap is automatically eliminated. Also, this converter, like its discrete-magnetic counterpart, can be made to operate as a boost converter, if the primary switches are purposely forced to have overlaping conduction intervals [13].

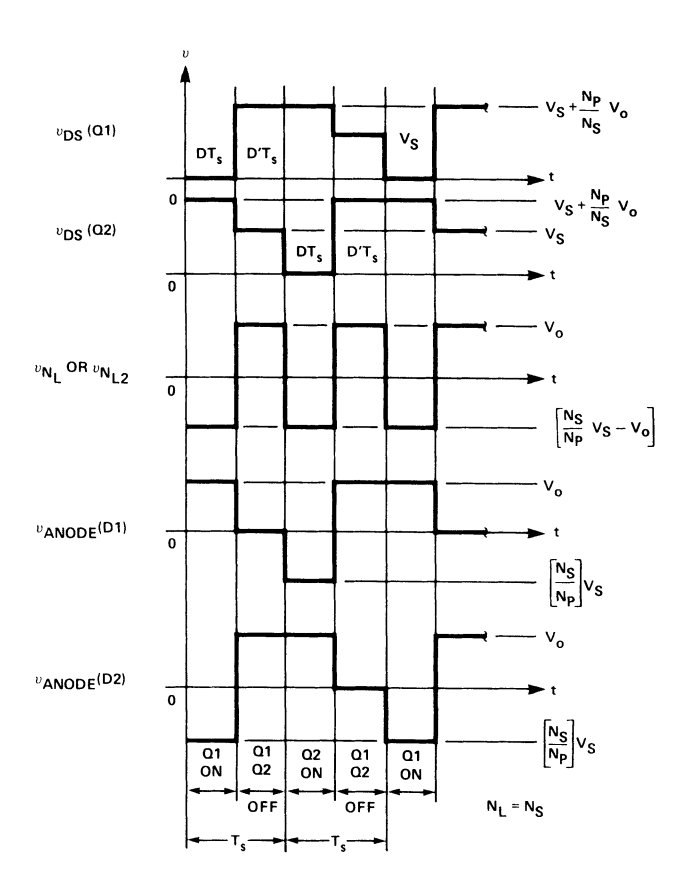


Figure 24 Voltage waveforms in the converters of Figure 22 (continuous mode).

8 SMALL-SIGNAL MODELING CONSIDERATIONS

Even though the magnetics of a buck or boost-derived converter have been magnetically integrated, modeling and analysis for stability and other dynamic studies is straight-forward, using proven techniques, such as the state-space averaging method [2]. All that is necessary is to derive an electric circuit model for the integrated-magnetic system, and then to add it in place of the magnetic in the converter topology. Following this, the normal procedures for deriving small-signal averaged models are followed, accounting for additional inductive elements [16] as presented by the integrated-magnetic arrangement.

For example, the averaged small-signal model for the integrated-magnetic version of the forward converter of Figure 13, using its equivalent electric-circuit topologie from Figure 16, is illustrated in Figure 25. Note that the averaged model accounts for all of the inductive elements of the electric-circuit model, as well as its isolation transformer. If we had chosen to add leakage inductances to the electric-circuit representations

in Figure 16, they could also have been easily accounted for in the equivalent small-signal model.

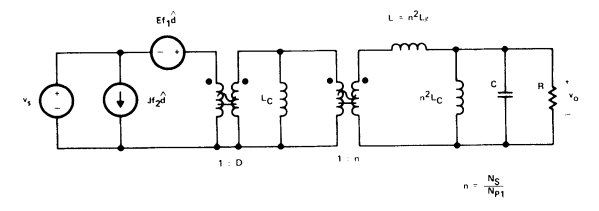
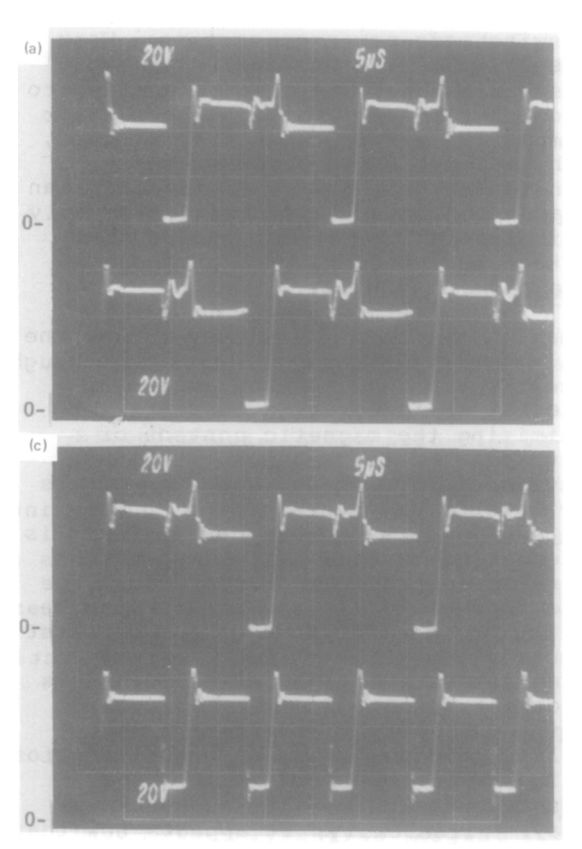


Figure 25 Averaged small-signal model of the integrated-magnetic forward converter of Figure 13.

9 LABORATORY INVESTIGATIONS

All of the integrated-magnetic versions of the various converters shown in this paper have been built and tested by the authors over the past two years. Major areas of interest for these empirical examinations were verification of expected DC voltage transfer functions and anticipated dynamic waveforms within the converters. In all cases, the results obtained were very close to those predicted.



Typical of the test results are the voltage waveforms taken for a low-power version of the integrated-magnetic Weinberg converter of Figure 22(b), snown in Figures 26(a) through (c). In this instance, the supply voltage was set at 40 VDC, and PWM duty cycles of Q1 and Q2 $\,$ manually adjusted to obtain an output voltage of 5VDC, across a load of 5 ohms and an output capacitor, C, of 100 microfarads. PWM clock frequency was set very close to 100KHz, resulting in a 50KHz switching frequency of each primary power switch. Also, to minimize voltage "spikes" produced by leakage inductances, small R-C snubbers (1.2K ohm + 0.01 uf) were added across each primary winding and across N_{L2}.

The integrated magnetic used for this particular experiment was composed of two joined Ferroxcube E625 E-cores, with each of their center legs ground to produce a total airgap length of 0.01". Three bobbins were then placed on each leg of the core structure, each with two sets of windings. Each winding set was composed of 30 turns of #20 AWG wire and 15 turns of #20 AWG wire. The completed magnetic was then connected into the converter arrangement of Figure 22(b), with

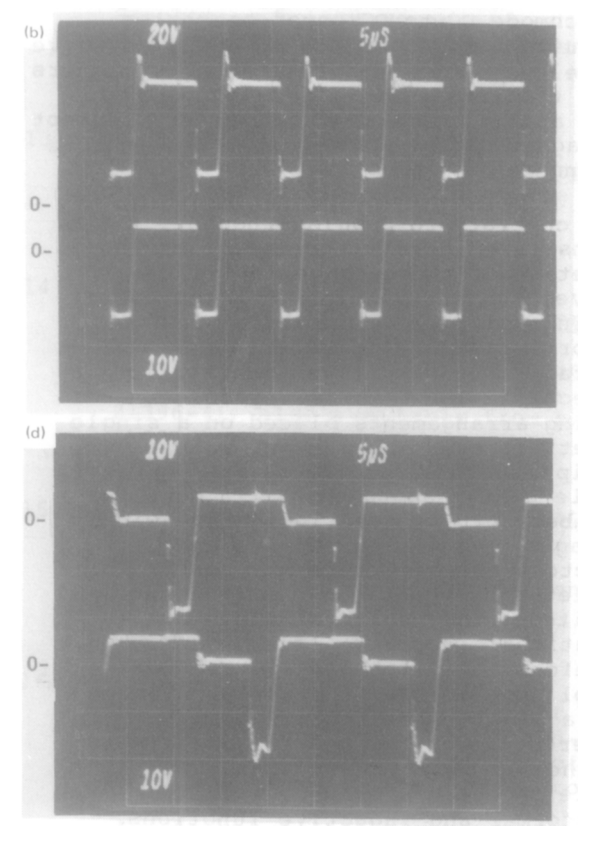


Figure 26 Breadboard test photos of voltages within the integrated-magnetic Weinberg converter of Figure 22(b).

windings phased as shown. Windings with 30 turns were used as primaries and for $N_{L\,1}$, while the 15-turn windings were used for the secondaries and for $N_{L\,2}$.

Using the relationships developed in Section 2, the inductance of the 15T center-leg winding was calculated to be about 1 mh for an airgap length of 0.01". Inductances of the primary windings on the outer legs were also calculated to be about 10 times that of this center-leg winding, confirming the earlier assumption that these latter inductances are indeed much larger in value.

Comparing the lab photos of Figure 26 to the ideal waveforms of Figure 24 expected in this design, we find that they closely match in all instances. Also, the observed duty cycle of each primary switch is in close agreement with that predicted earlier by (24) when correction is made for converter efficiency.

10 CONCLUDING REMARKS

In this paper, we have presented a broader and more general insight into integrated-magnetic concepts for switchmode DC-to-DC power converter circuits and, hopefully in doing so, have dispelled a common belief among designers that the transformers and inductors of buck and boost-derived converters can not be magnetically blended on a single core arrangement.

Also contrary to popular thought, the demonstrated ability to integrate the magnetics of these converters also removes the restriction that impressed winding voltages be completely proportional in all respects. general, this particular restriction is correct, if one thinks only in terms of winding arrangements placed on a single magnetic path. However, as we have seen, multiple-path arrangements are perfectly viable design approaches. It must be remembered that, even though the winding voltages of the transformers and inductors in converters may not be completely proportional in frequency and amplitude, they share a common operational property - flux change. Therefore, if relationships can be established between their flux changes from a knowledge of their position in a converter circuit, then it possible to use them to deductively synthesize a single magnetic system to house all transformer and inductive functions.

With integrated-magnetic versions of first-order buck and boost converters established, the possibility of magnetic integration of all of their family member topologies becomes immediately evident. Many of these possibilities are shown in [14], while others are still to be disclosed in the future. Although we have presented integrated-magnetic versions of single-output buck and boost converter arrangements, the idea is easily extended to accomodate multiple outputs, or multiple inputs as the case may be. This is easily done by the addition of more secondary or primary windings on appropriate core legs, together with contemporary switches and diodes.

In this paper, we have also shown methods whereby more windings can be added to inductive core paths to control input or output ripple current magnitudes, and significantly reduce them by proper internal and/or external magnetic means. Even though we have used single inductive paths in making this demonstration, it is also feasible to add more core legs with appropriate airgaps to the integrated—magnetic systems to control ripple current characteristics of contemporary windings, much in the same manner as was shown in [10] for the two inductors of a 'Cuk converter.

The discussion here has been restricted to switchmode power converters. Work presently in progress indicates that these techniques can also be applied to resonant converter circuits. Take for example the series resonant converter, with an inductor in series with the transformer primary. This inductor can be absorbed into the transformer simply by increasing the primary-secondary leakage inductance. This produces an integrated magnetic.

Finally, we conclude our paper with the following reflective thoughts. Although recent years have seen an increased interest in integration concepts for minimizing the magnetic content of converters or for enhancing their conversion properties, such techniques have historical roots, reaching back into the early years of this centruy. It is interesting to note that many advances in magnetic concepts for electronics were made in these earlier periods, with years following the introduction of the first electronic digital computer seeing little or no new work being continued in this important aspect of power electronics design. Shortly thereafter, a sad decline in educational opportunities for engineers in the field of practical magnetics design began, and continues today. Ironically, it appears now that magnetics could hold the key to achieving smaller and more efficient power conversion systems. As was noted in the introduction of this paper, it is truly a time of frustration and reflection for the power electronics engineer.

ACKNOWLEDGEMENTS

The authors would once again like to thank Morris Rauch for his help in constructing the breadboards of the various integrated-magnetic converters shown in this paper. Also, a special thank-you is sent to Colonel Wm. T. McLyman of CALTECH's Jet Propulsion Laboratory for constructing one of the integrated magnetics for the breadboards, and to the engineering directorate of Christie Electric Corporation for the use of their laboratory facilities during the breadboard testing efforts.

To J. Ceilo and H. Hoffman of IBM, we send a very special inspiration thankds for their exceptional 1971 patent concerning integrated magnetics for "push-pull" DC-to-DC power converter circuits.

REFERENCES

- [1] R. D. Middlebrook, "Reduction of Switching Ripple in Power Converters," Proceedings of the Sixth International PCI Conference, April 19-21, 1983, p. 6-14.
- [2] Slobodan Cuk, Modelling, Analysis, and Design of Switching Converters, Ph.D. Thesis, California Institute of Technology, Pasadena, CA, 1977.
- [3] Slobodan Cuk, "A New Zero-Ripple Switching DC-to-DC Converter and Integrated Magnetics," 1980 IEEE Power Electronics Specialists Conference Record, p. 12-32 (IEEE Publication 80CH1529-7 AES).
- [4] J. K. Watson, <u>Applications of Magnetism</u>, John Wiley and Sons, 1980.
- [5] C. Desoer and E. Kue, Basic Circuit Theory, McGraw Hill, 1969, p. 453-457.
- [6] G. B. Crouse, "Electrical Filter," U.S. Patent 1,920,948 (August 1, 1933).
- [7] S. Feng et.al., "Small-Capacitance Nondisapative Ripple Filters for DC Supplies, ." IEEE Transactions on Magnetics, Vol. MAG-6, No. 1, March, 1970.

- [8] G. E. Bloom and A. Eris,
 "Practical Design Considerations
 of a Multi-Output Cuk Converter,"
 1979 IEEE Power Electronics
 Specialists Conference Record, P.
 133-146 (IEEE Publication
 79CH1461-3 AES).
- [9] L. Rensink, Switching Regulator Configurations and Circuit Realizations, Ph.D. Thesis, California Institute of Technology, 1979.
- [10] Slobodan Cuk, "Analysis of Integrated Magnetics to Eliminate Current Ripple in Switching Converters," Proceedings of the Sixth International PCI Conference April, 1983, p. 361-386.
- [11] J. Cielo and H. Hoffman, "Combined Transformer and Indicator Device," U.S. Patent 3,553,620 (January 5, 1971).
- [12] Slobodan Cuk, "General Topological Properties of Switching Structures," 1979 Power Electronics Specialists Conference Record, p. 109-130 (IEEE Publication 79CH1461-3 AES).
- [13] Rudy Severns, "Techniques for Designing New Types of Switching Regulators," Proceedings of the International PCI Conference, September, 1979, paper 5.5.
- [14] G. E. Bloom and Rudy Severns,

 Modern DC-to-DC Switchmode Power

 Converter Circuits, to be

 published in 1984 by Van NostrandReinhold, Inc. (Catalog #0-44221396-4), also available from e/j
 BLOOM associates, 1312 Lovell
 Avenue, Arcadia, CA 91006.
- [15] A. H. Weinberg, "A Boost Regulator with a New Energy Transfer Principle," Proceedings of the 1974 Spacecraft Power Conversion Electronics Seminar (ESRO Publication SP-103).
- [16] R. D. Middlebrook, "Design Techniques for Preventing Input Filter Oscillations in Switched-Mode Regulators," Proceedings of POWERCON 5, May 1978, p. A3-1 to A3-16.
 - (17) L. Rensink, "Switching Regulator Configurations and Circuit Realizations" PHd. Dissertation, California Institute of Technology, 1980
 - (18) W. Polivka, "Applications of Magnetics to Problems In Switched-Mode Power Conversion" PHd, Dissertation, California Institute of Technology, February 1984